Parallel Accelerated Imaging of Alveolar Partial Pressure of Oxygen

Stephen J. Kadlecek[1], Yinan Xu[1], Kiarash Emami[1], Yi Xin[1], Puttisarn Mongkolwisetwara[1], Hooman Hamedani[1], Harrison McAdams[2], Masaru Ishii[3], and Rahim R. Rizi[1]

[1]*Radiology, University of Pennsylvania, Philadelphia, PA, United States,* [2]*Biological Basis of Behavior Program, University of Pennsylvania, Philadelphia, PA, United States,* [3]*Otolaryngology - Head and Neck Surgery, Johns Hopkins University, Baltimore, MD, United States*

INTRODUCTION: Hyperpolarized (HP) gas MRI has been applied to regional measurement of various pulmonary parameters, including the alveolar partial pressure of oxygen (P_AO_2). As it directly relates the fundamental function of the lung, effective P_AO_2 mapping would be a particularly interesting biomarker for lung disease diagnosis or staging. For a reliable measurement, however, a careful accounting of the interplay between RF- and oxygen-induced decay mechanisms is required. In this study, we investigate the potential for parallel imaging to more effectively decouple these two mechanisms, both to increase the fidelity of the oxygen map and to maximize subject tolerance, while understanding and minimizing any confounding effect of artifacts associated with accelerated image reconstruction. This project is based on earlier P_AO_2 imaging timing scheme optimization [1] and similarly makes use of computational models, phantoms, feasibility is testing in a healthy human.

METHODS: The acquisition schemes evaluated in this study are shown in **Figure 1**. Fig. 1a depicts the fully-sampled scheme in which the entire tolerable breath-hold (in this case, just over 10 seconds) is used for sampling to achieve acceptable resolution. The shorter accelerated acquisition time allowed comparison of three different timing schemes (1.b-d) and examination of the tradeoff between fewer, high flip-angle acquisitions (1.b) and acquisition of more time-points (1.d). A fully-sampled image of a human lung and the associated P_AO_2 and flip angle (α) maps were used as the best available 'ground truth' for computationally comparing the accuracy and precision of the parallel accelerated oxygen mapping process to that of the full *k*-space sampling. The simulation consisted of three parts: *k*-sampling of the original spin-density images in presence of O_2 and RF decay effects, image reconstruction using various acceleration factors and reconstructions, and the P_AO_2 mapping process using the reconstructed images. Phantom experiments used a Tedlar bag filled with $^3He+N_2+O_2$ gas mixture and were conducted in order to verify trends uncovered by the simulation and to assess experimental error. Human experiments consisted of one healthy human subject who in a five-minute interval underwent two different P_AO_2 imaging schemes: the fully-sampled and undersampled modes 1.a and 1.b (the latter was chosen based on its performance in phantom and simulation studies). All experiments were performed on a Siemens Sonata 1.5-T MRI system with a commercial volume transmit, 8-channel receive phased array RF Coil (Stark Contrast, Germany). The transmit coil was saddle-shaped, 45 cm long and 35 cm wide, and both coils were tuned to the ^3He resonance frequency of 48.48 MHz. The phantom experiments utilized a gradient echo imaging pulse sequence with Cartesian sampling and the following parameters: FOV=30×30cm^2, TR/TE=6.8/3.25ms, and MS=64×64. Human imaging: FOV=40×40cm^2, 6 slices with anterior-to-posterior ordering, ST=20mm, TR/TE=6.8/3.25ms, and MS=64×64. For both the phantom and human studies shown, GRAPPA with an acceleration factor of 4 and 16 auto-calibration lines was used [2].

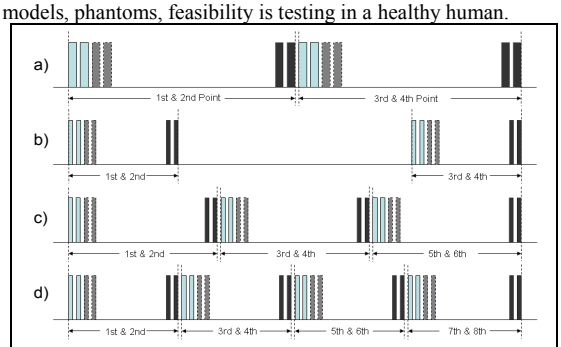

Figure 1. Diagram of the various acquisitions schemes performed in this study; fully sampled (a) and three accelerated schemes (b-d).

RESULTS: Figure 2 shows an example set of simulation results representative of the conditions encountered in a human experiment, in this case at a low average S/N of 20, which highlights the advantage of the accelerated scheme. Acceleration yields a greater overall S/N due to higher flip-angle and a correspondingly reduced deviation from the assumed ground truth. **Figure 3** summarizes phantom experiments which confirm this effect; repeated measurements in a bag with known pO_2 show a reduced average deviation (0.1% vs 5.0% for full sampling) and distribution width (7.1 vs 10.1% for full sampling) when using the four-point accelerated scheme of 1.b (red). For the human experiment, **Figure 4** shows the P_AO_2 maps from two different 4-point acquisition schemes with full *k*-space acquisition (α =5°) and accelerated acquisition (α =7°), numerical results for which are highlighted in the figure table.

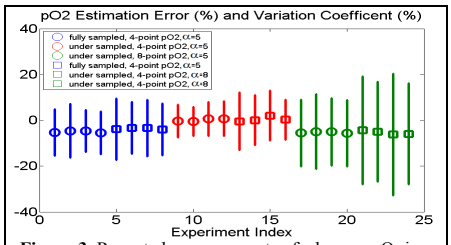

Figure 3. Repeated measurements of a known pO_2 in a tedlar bag using full *k*-space sampling (blue), the 4-point accelerated scheme (red, 1.b) and the 8-point scheme (green, 1.d).

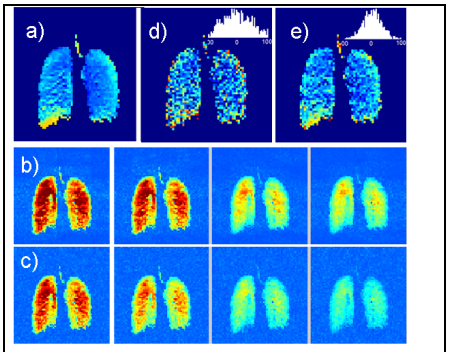

Figure 2. Simulation results, representative of the human experiments with S/N=20. Assumed ground truth signal intensity and P_AO_2 (a) is reconstructed from an undersampled (b) or fully sampled (c) image series according to schemes 1.a-b. The higher flip-angle and longer time-base of the accelerated scheme yields a reduced deviation (e, histogram insert).

DISCUSSION AND CONCLUSION: All three comparisons suggest that P_AO_2 mapping can be made more accurate by using an accelerated imaging scheme, minimizing both the bias of the mean and the deviation from the true spatial pattern of P_AO_2. On the other hand, acquiring additional images during the time delay opened up by the reduced-duration accelerated imaging (schemes 1.c-d) does not appear to benefit P_AO_2 estimation. One reason for the superiority of the accelerated scheme is that it distributes the fixed magnetization budget among a smaller number of excitations, concentrated toward the center of *k*-space, thereby maximizing S/N. In addition, it achieves the widest possible temporal separation between images within the subject-imposed breath-hold constraint. Three features are apparent from the human results: a strong gravity-induced gradient independent of imaging scheme, visual consistency between the schemes, and an overall narrower P_AO_2 distribution obtained from accelerated acquisitions, suggestive of reduced deviation from a (likely fairly uniform) true P_AO_2 distribution. It remains important, however, to account for various potential sources of error, including the effects of diffusion and gas flow, which may be easier if additional images are acquired and warrants further investigation in a larger number of subjects. The results so far suggest that parallel accelerated imaging, and presumably other image acceleration schemes, can provide a better platform for P_AO_2 mapping compared to full *k*-space sampling through enhancement of O_2-induced contrast, and spatial artifacts or blurring introduced by acceleration do not appear to adversely affect the estimate. Notably, simulation results suggest that the advantages of parallel, accelerated imaging disappear in the limit of high S/N in each image, but will be even more pronounced when S/N is especially limited, e.g., in hyperpolarized ^{129}Xe imaging.

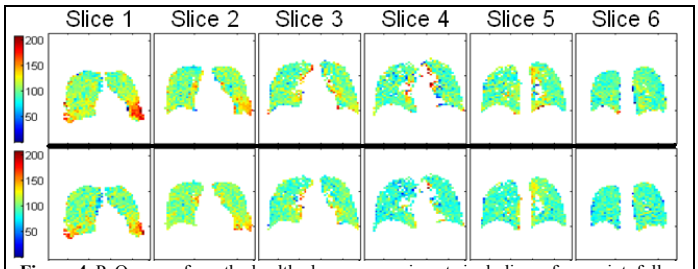

Figure 4. P_AO_2 maps from the healthy human experiments including a four-point, full *k*-space acquisition with nominal flip-angle of 5° (top) and the four-point, accelerated acquisition using a nominal flip-angle of 7° (bottom). The corresponding slice variation coefficients are (0.27, 0.23, 0.28, 0.29, 0.25, 0.21, slice 1-6, fully sampled) and (0.22, 0.19, 0.20, 0.25, 0.20, 0.19, slice 1-6, accelerated). Each distribution width is reduced, suggesting greater accuracy through reduction of S/N-induced uncertainty.

REFERENCES

1. Fischer MC, et al. Magn Reson Med 2004;52(4):766-773; 2. Griswold MA, et al. Magn Reson Med 2002;47(6):1202-1210.